



Semnan University

# Mechanics of Advanced Composite Structures

journal homepage: <http://MACS.journals.semnan.ac.ir>

## Functionally Graded Piezoelectric Plates in Cylindrical Bending by Semi-analytical Approach

S. Sawarkar <sup>a\*</sup>, S. Pendhari <sup>b</sup><sup>a</sup> Department of Civil Engineering, Pimpri Chinchwad College of Engineering & Research, Pune – 412101, India<sup>b</sup> Department of Structural Engineering, Veermata Jijabai Technological Institute, Mumbai – 400019, India

### KEYWORDS

Static analysis;  
Semi-analytical method;  
Functionally graded  
piezoelectric material;  
2-D domain.

### ABSTRACT

A simply supported (SS) functionally graded piezoelectric material (FGPM) plate in a 2D domain has been analyzed for stress and displacement by a Semi-analytical approach. In-plane variation in stresses and displacements is assumed to be trigonometric. The elasticity approach is used and no simplifying assumption is made on the stress and displacement fields in the through-thickness direction. The FGPM plate is subjected to a transverse electro-mechanical load whose intensity remains constant in the out-of-plane direction. Thus, the plate is under plane stress and plane strain conditions of elasticity. Exponential law or power law has been considered for smooth gradation of material properties in the through-thickness direction. The formulation is a set of first-ordered ordinary differential equations (ODE), which has been solved using numerical integration. Exact outcomes in the literature have been used to correlate and validate the present model results. Additional investigation has been carried out on FGPM plates and beams and results are provided for future reference.

## 1. Introduction

Stress and displacement analysis of smart materials remain to be an active area of research to date. Smart materials are formed with an elastic substrate having embedded or attached patches of piezoelectric materials. By virtue of actuation, piezo-materials undergo deformation under the applied electric field and by virtue of sensing, produce an electric charge on deforming mechanically. This ability of inter-conversion of mechanical and electrical energy of piezo-materials is judiciously used to develop self-controlling, self-governing smart materials.

FGPM is a relatively new addition to this class of materials in which, material elastic and electric properties are changed gradually, generally in the thickness direction. These eliminate the development of stress-offsets at the interfaces and reduce the threat of de-lamination, which is typically observed in layered composites.

Smart materials find numerous applications in every walk of engineering, including aerospace

and aeronautical industry, robotics, and medical instrumentation. These high-end applications demand accurate and involved analysis and it is essential to have a robust, versatile, and computationally inexpensive analysis tool.

Researchers have proposed several analytical and numerical solutions based on exact and approximate theories. A functionally graded piezoelectric plate loaded with electro-mechanical loading in the 2D field has been analyzed by Lu et al. [1] with the help of elasticity solutions. Similarly, Lu et al. [2] have analyzed an all-around simply supported FGPM plate for the exact solution. Xiang and Shi [3] have presented a static analysis of the FGPM sandwich cantilever using Airy's stress function. Mikaeeli and Behjat [4] have used the three-dimensional element-free Galerkin method to investigate the static behavior of thick functionally graded piezoelectric plates. Kulikov and Plotnikova [5] have used the sampling surfaces method for the exact analysis of thick and thin FG piezoelectric laminated plates with specified accuracy. Exact

\* Corresponding author. Tel.: +91-8850159922  
E-mail address: [sameer.sawarkar@pccoer.in](mailto:sameer.sawarkar@pccoer.in)

solutions for FGPM plates have also been provided by Lim and He [6], Reddy and Cheng [7], and Zhong and Shang [8].

Exact solutions, though invaluable, are often difficult to obtain due to the mathematical complexities involved in the solution techniques. Thus, efforts are made to put forth approximate models based upon equivalent single-layer theory or layer-wise theories. A large quantum of literature is found on approximate analysis of FGPM plates, including those from Almajid et al. [9], Joshi et al. [10], Taya et al. [11], Zhong and Yu [12], Wu et al. [13], Loja et al. [14], Li et al. [15], Chuaqui and Roque [16], Nourmohammadi and Behjat [17], Behjat and Khoshnavan [18], Raissi H. [19], Raissi et al. [20, 21] among others.

In addition to the static analysis, extensive work has been carried out by the researchers on vibrations and wave propagation in Functionally Graded Material (FGM) plates and FGPM plates, a significant contribution coming from Song and Luo [22], Mazzotti et al. [23], Li et al. [24], Li and Han [25], Li et al. [26], Vinh and Tounsi [27], Tahir et al. [28], Rachid et al. [29], Habib et al. [30], Boufia et al. [31], Zaitoun et al. [32], Mudhaffar et al. [33], Kouider et al. [34], Merazka et al. [35], Hachemi et al. [36] and Bakoura et al. [37].

The present paper gives a semi-analytical model for the stress and displacement analysis of a simply supported FGPM plate in cylindrical bending. In-plane displacement ( $u$ ), transverse displacement ( $w$ ), transverse normal stress ( $\sigma_z$ ), transverse shear stress ( $\tau_{xz}$ ), electric potential ( $\phi$ ) and transverse electric displacement ( $D_z$ ) are considered as primary variables. An FGPM plate acted upon by electro-mechanical loading is formulated as a mixed two-point boundary value problem (BVP) in the interval  $-h/2 \leq z \leq h/2$ , with half of the variables specified at the edges  $z = \pm h/2$ . In-plane variation in primary variables is assumed to be trigonometric, keeping consistent with the relevant electro-elastic boundary conditions (BCs). The Semi-analytical model developed with algebraic manipulation of governing elasticity equations is a set of first-ordered ordinary differential equations, which can be easily solved using numerical integration. The model is simple, mixed, versatile, accurate, and computationally inexpensive. However, this approach is suitable only for simply supported or clamped-clamped BCs and not for any arbitrary BCs.

## 2. Mathematical Formulation

An FGPM plate with dimensions  $a$ ,  $b$ , and  $h$  in  $x$ ,  $y$ , and  $z$  directions respectively, has been considered. The plate's mid-plane is assumed to be the reference  $x$ - $y$  plane and the transverse axis

is in the  $z$ -direction (Figure 1). Edges at  $x = 0, a$  are diaphragm supported and grounded to zero potential. The top layer of the plate is loaded with transverse mechanical and electrical loading, which is independent of the  $y$ -direction. Condition of elasticity shall be considered as of plane strain or plane stress depending upon the dimension  $b$  being extremely long or extremely short.

The material properties of FGPM are assumed to vary in the depth direction as;

$$C_{ij} = f(z)C_{ij}^0, e_{ij} = f(z)e_{ij}^0, g_{ij} = f(z)g_{ij}^0 \quad (1)$$

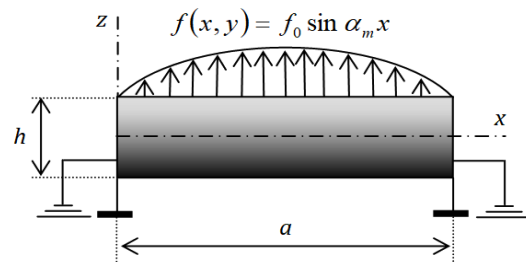


Fig. 1. Simply Supported FGPM Plate

where,  $C_{ij}$ ,  $e_{ij}$  and  $g_{ij}$  are the values at any arbitrary depth and  $C_{ij}^0, e_{ij}^0, g_{ij}^0$  are the available reference values. Poisson's ratios  $\nu_{ij}$  are invariants. Gradation  $f(z)$  is either exponential law or power law, which is popularly used in literature.

Coupled elastic and electric fields equations given by Tirsten [38] are;

$$\begin{aligned} \{\sigma\} &= [C^E]\{\varepsilon\} - [e]\{E\}, \\ \{D\} &= [e]^T\{\varepsilon\} + [g^S]\{E\} \end{aligned} \quad (2)$$

2D elasticity equilibrium equations and strain-displacement equations are;

$$\begin{aligned} \frac{\partial \sigma_x}{\partial x} + \frac{\partial \tau_{zx}}{\partial z} + B_x &= 0, \\ \frac{\partial \tau_{xz}}{\partial x} + \frac{\partial \sigma_z}{\partial z} + B_z &= 0 \end{aligned} \quad (3)$$

$$\varepsilon_x = \frac{\partial u}{\partial x}, \varepsilon_z = \frac{\partial w}{\partial z}, \gamma_{xz} = \frac{\partial u}{\partial z} + \frac{\partial w}{\partial x} \quad (4)$$

Maxwell [39] has given a charge equilibrium equation in a 2D domain as;

$$\frac{\partial D_x}{\partial x} + \frac{\partial D_z}{\partial z} = 0 \quad (5)$$

The vectors and matrices appearing in Eqs. (2) are given in the Appendix.

Equations (2)-(5) consist of inter-dependent 11 unknowns, viz.  $u, w, \varepsilon_x, \varepsilon_z, \gamma_{xz}, \sigma_x, \sigma_z, \tau_{xz}, D_x, D_z$  and  $\phi$  in 11 equations. After an algebraic simplification of the above set of equations, a set of partial differential equations (PDEs) involving

only six chosen primary variables and the gradation function  $f(z)$  is obtained as;

$$\begin{aligned} \frac{\partial u}{\partial z} &= \frac{\tau_{xz}}{f(z)C_{55}^0} - \frac{e_{15}^0}{C_{55}^0} \frac{\partial \phi}{\partial x} - \frac{\partial w}{\partial x} \\ \frac{\partial w}{\partial z} &= \frac{1}{f(z)} \left( \frac{g_{33}^0}{C_{33}^0 g_{33}^0 + e_{33}^0 e_{33}^0} \right) \sigma_z \\ &+ \frac{1}{f(z)} \left( \frac{e_{33}^0}{C_{33}^0 g_{33}^0 + e_{33}^0 e_{33}^0} \right) D_z \\ &- \left( \frac{g_{33}^0 C_{31}^0 + e_{33}^0 e_{31}^0}{C_{33}^0 g_{33}^0 + e_{33}^0 e_{33}^0} \right) \frac{\partial u}{\partial x} \\ \frac{\partial \phi}{\partial z} &= \frac{1}{f(z)} \left( \frac{e_{33}^0}{C_{33}^0 g_{33}^0 + e_{33}^0 e_{33}^0} \right) \sigma_z \\ &- \frac{1}{f(z)} \left( \frac{C_{33}^0}{C_{33}^0 g_{33}^0 + e_{33}^0 e_{33}^0} \right) D_z \\ &+ \left( \frac{C_{33}^0 e_{31}^0 - e_{33}^0 C_{31}^0}{C_{33}^0 g_{33}^0 + e_{33}^0 e_{33}^0} \right) \frac{\partial u}{\partial x} \\ \frac{\partial \tau_{xz}}{\partial z} &= -f(z) \left( \frac{C_{11}^0}{C_{33}^0 g_{33}^0 + e_{33}^0 e_{33}^0} - \frac{C_{13}^0 g_{33}^0 C_{31}^0 + e_{33}^0 C_{13}^0 e_{31}^0}{C_{33}^0 g_{33}^0 + e_{33}^0 e_{33}^0} \right) \frac{\partial^2 u}{\partial x^2} \\ &+ \left( \frac{e_{31}^0 C_{33}^0 e_{31}^0 - e_{31}^0 C_{31}^0 e_{33}^0}{C_{33}^0 g_{33}^0 + e_{33}^0 e_{33}^0} \right) \frac{\partial \sigma_z}{\partial x} \\ &- \left( \frac{C_{13}^0 g_{33}^0 + e_{31}^0 e_{33}^0}{C_{33}^0 g_{33}^0 + e_{33}^0 e_{33}^0} \right) \frac{\partial \sigma_z}{\partial x} \\ &- \left( \frac{C_{13}^0 e_{33}^0 - e_{31}^0 C_{33}^0}{C_{33}^0 g_{33}^0 + e_{33}^0 e_{33}^0} \right) \frac{\partial D_z}{\partial x} - B_x \\ \frac{\partial \sigma_z}{\partial z} &= -\frac{\partial \tau_{xz}}{\partial x} - B_z \\ \frac{\partial D_z}{\partial z} &= -\frac{e_{15}^0}{C_{55}^0} \frac{\partial \tau_{xz}}{\partial x} + f(z) \left( \frac{e_{15}^0 e_{15}^0}{C_{55}^0} + g_{11}^0 \right) \frac{\partial^2 \phi}{\partial x^2} \end{aligned} \tag{6}$$

Kantorovich [40] approach is used to convert the obtained set of PDEs into a set of ordinary differential equations (ODEs). The in-plane variation in displacement field and stress field is considered to be trigonometric, satisfying elastic and electric boundary conditions at  $x = 0, a$ , as;

$$\begin{aligned} \begin{Bmatrix} u(x, z) \\ \tau_{xz}(x, z) \end{Bmatrix} &= \sum_m \begin{Bmatrix} u_m(z) \\ \tau_{xzm}(z) \end{Bmatrix} \cos \alpha_m x \\ \begin{Bmatrix} w(x, z) \\ \sigma_z(x, z) \\ D_z(x, z) \end{Bmatrix} &= \sum_m \begin{Bmatrix} w_m(z) \\ \sigma_{zm}(z) \\ D_{zm}(z) \end{Bmatrix} \sin \alpha_m x \end{aligned} \tag{7}$$

where  $\alpha_m = \frac{m\pi}{a}$ ,  $m = 1, 3, 5, \dots$

The transverse mechanical load  $p(x, z)$  and electrostatic potential  $\phi(x, z)$  are represented using Fourier series to facilitate the application of an arbitrarily distributed load as;

$$\begin{Bmatrix} p(x, z) \\ \phi(x, z) \end{Bmatrix} = \sum_m \begin{Bmatrix} p_{0m}(z) \\ \phi_{0m}(z) \end{Bmatrix} \sin \alpha_m x \tag{8}$$

Substituting Eqs. (7), (8) and the derivatives into Eqs. (6), a set of first-order ODEs containing primary dependent variables and the gradation function  $f(z)$  is obtained as;

$$\begin{aligned} \frac{d}{dz} \begin{Bmatrix} u_m(z) \\ w_m(z) \\ \phi_m(z) \\ \tau_{xzm}(z) \\ \sigma_{zm}(z) \\ D_{zm}(z) \end{Bmatrix} &= \begin{bmatrix} Q_{11} & Q_{12} & Q_{13} & Q_{14} & Q_{15} & Q_{16} \\ Q_{21} & Q_{22} & Q_{23} & Q_{24} & Q_{25} & Q_{26} \\ Q_{31} & Q_{32} & Q_{33} & Q_{34} & Q_{35} & Q_{36} \\ Q_{41} & Q_{42} & Q_{43} & Q_{44} & Q_{45} & Q_{46} \\ Q_{51} & Q_{52} & Q_{53} & Q_{54} & Q_{55} & Q_{56} \\ Q_{61} & Q_{62} & Q_{63} & Q_{64} & Q_{65} & Q_{66} \end{bmatrix} \begin{Bmatrix} u_m(z) \\ w_m(z) \\ \phi_m(z) \\ \tau_{xzm}(z) \\ \sigma_{zm}(z) \\ D_{zm}(z) \end{Bmatrix} \\ &+ \begin{Bmatrix} 0 \\ 0 \\ 0 \\ -B_x \\ -B_z \\ 0 \end{Bmatrix} \end{aligned} \tag{9}$$

The electro-elastic coefficients  $Q_{11}-Q_{66}$  in Eqs. (9) are given in the Appendix.

The above Eqs. (9) show the mixed two-point BVP in the realm  $-h/2 \leq z \leq h/2$ , with stress components and transverse electric displacement (open circuit condition) or electric potential (closed-circuit condition) known at the upper and lower faces of the plate. The secondary variables are represented in the form of primary variables as;

$$\begin{aligned} \sigma_x &= \sum_m f(z) \begin{Bmatrix} -C_{11}^0 \alpha_m u_{mn}(z) \\ C_{13}^0 \frac{dw_{mn}(z)}{dz} \\ + e_{31}^0 \frac{d\phi_{mn}(z)}{dz} \end{Bmatrix} \sin \alpha_m x \\ D_x &= \sum_m f(z) \begin{Bmatrix} e_{15}^0 \frac{du_{mn}(z)}{dz} \\ + e_{15}^0 \alpha_m w_{mn}(z) \\ - g_{11}^0 \alpha_m \phi_{mn}(z) \end{Bmatrix} \cos \alpha_m x \end{aligned} \tag{10}$$

### 3. Solution Methodology

Numerical integration is used to obtain solutions to Eq.s (9). The BVP is converted into an initial value problem (IVP) [41] and the shooting approach is used to solve the ODEs in Eq. (9). The solution methodology has been discussed in detail elsewhere [42] and is not repeated here.

### 4. Numerical Results and Discussion

Numerical investigation using Semi-analytical methodology is discussed below. A simply supported infinite FGPM plate and an FGPM/Homogeneous bi-layered laminate under electro-mechanical loading have been investigated to validate the model. Additionally, a few examples of FGPM and hybrid beams of different piezo materials have been addressed.

#### Example 1

An infinitely long PZT-4 based FGPM simply supported plate has been considered. Elastic and electric properties of the plate are considered to vary exponentially in the depth direction as;

$$\begin{aligned} C_{ijkl} &= C_{ijkl}^0 e^{\beta z}, e_{ijkl} = e_{ijkl}^0 e^{\beta z}, \\ g_{ijkl} &= g_{ijkl}^0 e^{\beta z} \end{aligned} \quad (11)$$

where  $\beta = -1, -0.5, 0, 0.5, 1$  is the material grading constant. Reference values  $C_{ijkl}^0, e_{ijkl}^0$  and  $g_{ijkl}^0$  are expressed in Table 1. The plate is considered to be thick with an aspect ratio of  $a/h = 1$ . Firstly, the plate is loaded by a mechanical load;

$p = 1 \sin\left(\frac{\pi x}{a}\right)$  with upper and lower faces held at zero potential. Secondly, it is exposed to electric load;  $\phi = 1 \sin\left(\frac{\pi x}{a}\right)$  with no applied stresses at the

upper and lower faces. Loading being independent of  $y$ -direction, the FGPM plate is in plane strain condition of elasticity. Comparison of present theory (PT) results of through-thickness variation in displacements and stresses evaluated at section  $x = 0.25a$  with analytical results given by Lu et al. [1] is illustrated for a sensory plate in Figure 2 and for an actuating plate in Figure 3. Present results match the exact result for both, the sensory and the actuating plates.

**Table 1.** Material Properties (<sup>a</sup>Reference [1], <sup>b</sup>Reference [43] <sup>c</sup>Reference [44])

Material	Properties
PZT-4 <sup>a</sup>	$C_{11} = 139$ (GPa), $C_{13} = 74.3$ , $C_{33} = 115, C_{55} = 25.6$ $e_{31} = -5.2$ (C/m <sup>2</sup> ), $e_{33} = 15.1, e_{15} = 12.7$ $g_{11} = 1.306 \times 10^{-8}$ (F/m), $g_{33} = 1.151 \times 10^{-8}$
PVDF <sup>b</sup>	$E_1 = 237$ (GPa), $E_3 = 10.5$ , $G_{44} = 2.15, G_{55} = 4.4, G_{66} = 6.43$ $\nu_{12} = 0.154, \nu_{13} = 0.178$ , $\nu_{23} = 0.177$ $e_{31} = -0.13$ (C/m <sup>2</sup> ), $e_{33} = -0.28, e_{15} = -0.01$ $\epsilon_{11}/\epsilon_0 = 12.5, \epsilon_{33}/\epsilon_0 = 11.98$
Ni <sup>c</sup>	$Y = 199.5$ GPa, $\nu = 0.3$
Al <sub>2</sub> O <sub>3</sub> <sup>c</sup>	$Y = 393$ GPa, $\nu = 0.25$
PZT-5A <sup>c</sup>	$Y_1 = 61$ (GPa), $Y_2 = 61, Y_3 = 53.2$ , $G_{44} = 22.6, G_{55} = 21.1, G_{66} = 21.1$ $\nu_{12} = 0.35, \nu_{13} = 0.38, \nu_{23} = 0.38$ $d_{31} = -171 \times 10^{-12}$ (m/V), $d_{33} = 374 \times 10^{-12}$ , $e_{15} = 584 \times 10^{-12}$ $g_{11} = 1.53 \times 10^{-8}$ (F/m), $g_{33} = 1.5 \times 10^{-8}$

It can be observed for the actuating plate in Figure 3(a) and (b) that change in material grading constant  $\beta$  does not affect in-plane displacement ( $u$ ) and transverse displacement ( $w$ ) to any large extent. However, a considerable increase in the value of transverse normal stress ( $\sigma_z$ ) and transverse shear stress ( $\tau_{xz}$ ) is observed (Figure 3(c) and (d)) with the increase in value of  $\beta$ . Thus, a grading stiff ( $\beta > 0$ ) material may fail under large electric force. On the other hand, a grading soft ( $\beta < 0$ ) material may effectively reduce the stresses under electric load. Figures 2 and 3 show that in sensory and actuating plates, the transverse displacement ( $w$ ) does not vary linearly through the depth, as assumed in a few approximate 2D plate theories. Further, the grading soft material shows significant non-linearity in  $w$  compared to the grading stiff material. Thus, for a grading soft FGPM plate, the assumption of linear variation in  $w$  may lead to a considerable error.

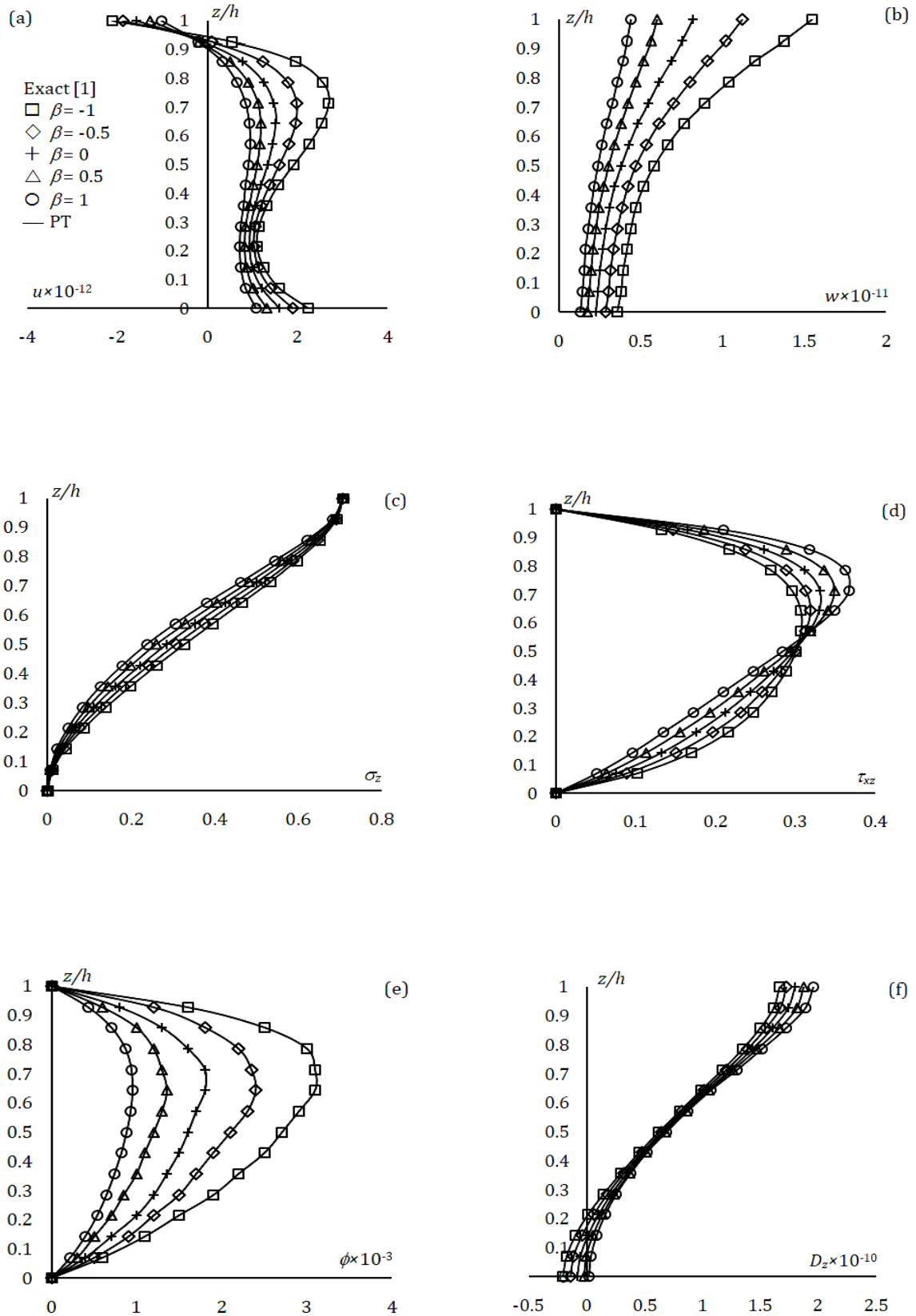


**Fig. 2.** Through-thickness variation in functionally graded PZT-4 sensory plate in (a) in-plane displacement, (b) transverse displacement, (c) transverse normal stress, (d) transverse shear stress, (e) induced electric potential, (f) transverse electric displacement

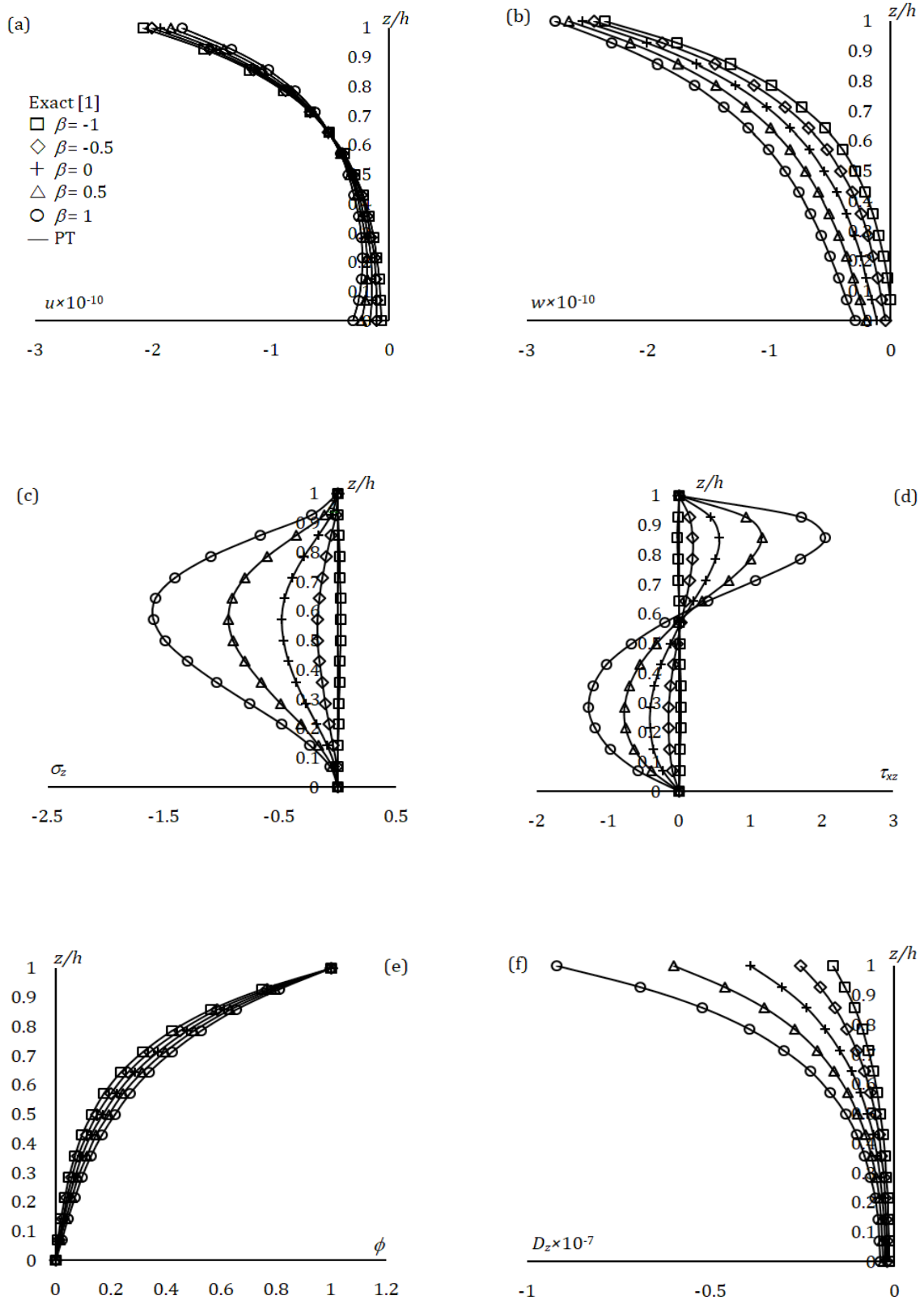


Fig. 3. Through-thickness variation in functionally gradient PZT-4 actuating plate in (a) in-plane displacement, (b) transverse displacement, (c) transverse normal stress, (d) transverse shear stress, (e) applied electric potential, (f) transverse electric displacement

### Example 2

A two-layered infinite simply supported FGPM/Homogeneous piezoelectric plate with overall thickness  $h$  in cylindrical bending is considered. The lower layer of thickness  $h_1$  is a homogeneous PZT-4 piezoelectric material with constant material properties (given in Table 1) and the upper layer of thickness  $(h - h_1)$  is a PZT-4 based FGPM. The elastic and electric properties in the upper FGPM layer vary as per the exponential law;

$$\begin{aligned} C_{ijkl} &= C_{ijkl}^0 e^{\beta(z-h_1)}, \quad e_{ijkl} = e_{ijkl}^0 e^{\beta(z-h_1)}, \\ g_{ijkl} &= g_{ijkl}^0 e^{\beta(z-h_1)} \end{aligned} \quad (12)$$

where  $\beta = -1, -0.5, 0, 0.5, 1$  is material gradient. The thickness of homogeneous layer  $h_1$  is considered to be  $0.2h$  and  $0.8h$ . The laminate is subjected to two loading cases; mechanical singly sinusoidal load at the top surface with electric displacement  $D_z$  at top and bottom zero and electric singly sinusoidal load at the top surface with traction-free faces. A comparison of through-thickness variation in stresses and displacements evaluated at a section  $x = 0.25a$  with exact solutions given by Lu et al. [1] is expressed in Figure 4 for the sensory plate and in Figure 5 for actuating plate.

Figure 4 shows that as the thickness of the FGPM layer decreases from  $0.8h$  to  $0.2h$ , the through-thickness variation curves of in-plane displacement ( $u$ ), transverse displacement ( $w$ ), transverse normal stress ( $\sigma_z$ ) for grading stiff ( $\beta > 0$ ) material and grading soft ( $\beta < 0$ ) material converge to corresponding curves for homogeneous ( $\beta = 0$ ) material. It can thus be observed that in the case of a sensory plate under mechanical loading, stresses and displacements may be restricted by using a suitable gradation factor, as well as by providing an appropriate thickness of the FGPM layer. However, in the case of actuating plates with an FGPM layer of  $0.2h$  thickness (Figure 5), curves for the transverse normal stress ( $\sigma_z$ ) in grading stiff and grading soft materials do not show any convergence towards those with the homogeneous material, indicating that the gradation factor  $\beta$  plays a very vital role in actuating plate under electric load and that

even a relatively thin layer of FGPM can have a distinct effect on stresses in the bi-layered plate.

### Example 3

A simply supported moderately thick ( $a/h = 10$ ) beam made up of functionally graded PVDF is considered. The material properties are assumed to vary exponentially as;

$$\begin{aligned} C_{ijkl} &= C_{ijkl}^0 e^{\beta z/h}, \quad e_{ijkl} = e_{ijkl}^0 e^{\beta z/h}, \\ g_{ijkl} &= g_{ijkl}^0 e^{\beta z/h} \end{aligned} \quad (13)$$

where the material grading constant  $\beta = -1, -0.5, 0, 0.5, 1$ . Reference values of  $C_{ijkl}^0, e_{ijkl}^0, g_{ijkl}^0$  are taken from Helinger et al. [43] and given in Table 1. The sensory beam is subjected to sinusoidal mechanical load with unit intensity. The actuating beam is subjected to sinusoidal electric load, again with unit intensity. Values of the entities at salient points are given in Table 2 for the sensory beam and in Table 3 for actuating beam, which may be used as benchmark results.

### Example 4

The beam in Example 3 is re-investigated for its response to uniformly distributed mechanical and electric load applied at the top face. Fourier coefficients  $p_0$  and  $\phi_0$  in Eqs. 8 are taken as  $\frac{4}{m\pi}$

where  $m = 1, 3, 5, \dots$  is varied. The solution is obtained by applying the Runge-Kutta Method of solving the IVP and convergence is observed to reach in about twenty iterations. Values of stresses and displacements at salient points are given in Table 4 for a sensory beam and in Table 5 for actuating beam for future reference.

Results indicate that in-plane displacement ( $u$ ) and transverse displacement ( $w$ ) at the top surface in the case of grading stiff beam are considerably small as compared to grading soft beam. This is observed in actuating as well as sensory beam. However, as the stiff portion of the FGPM beam absorbs more stresses, the in-plane stresses ( $\sigma_x$ ) at the top surface are much larger in grading stiff beam as compared to grading soft beam.

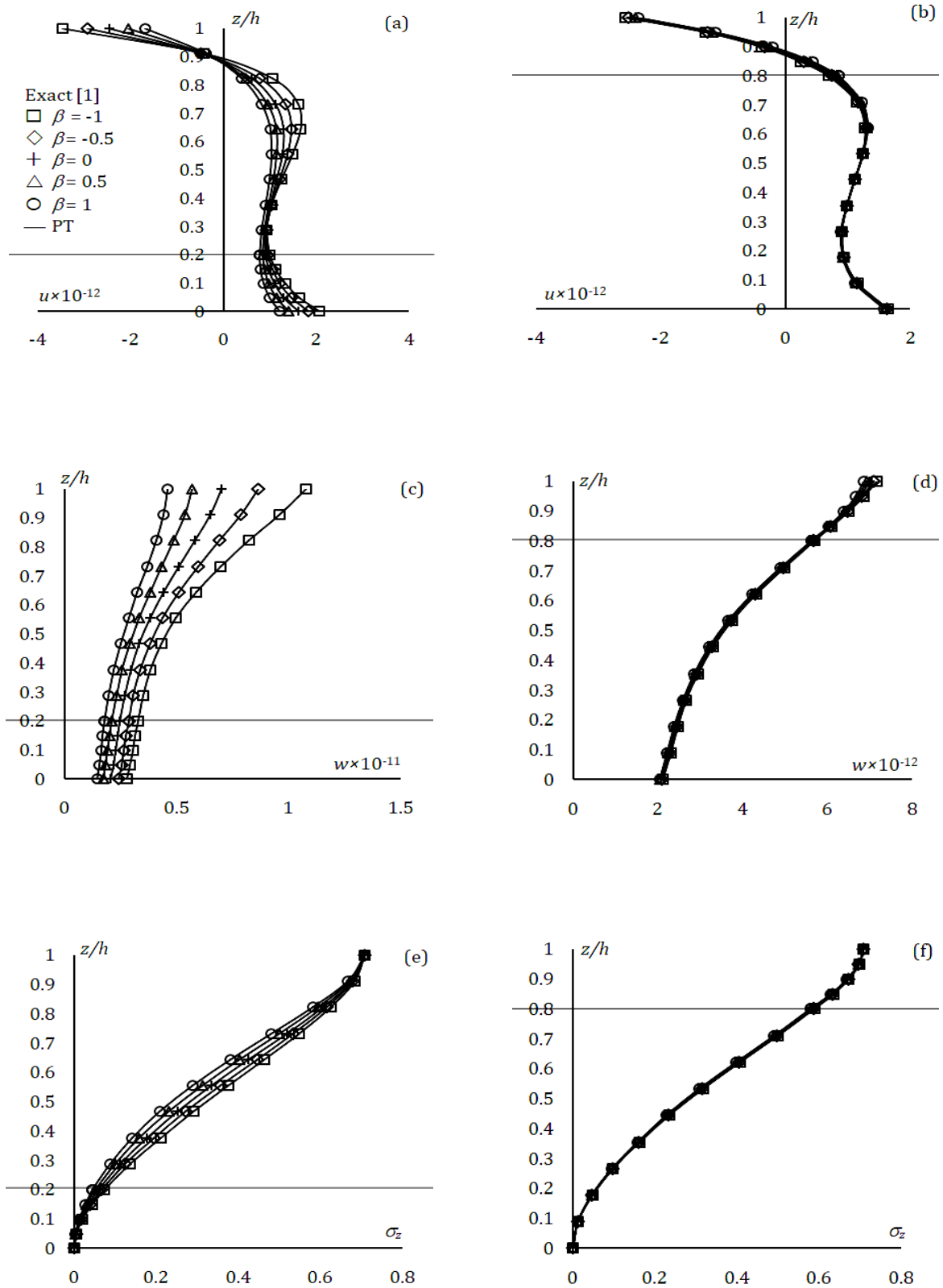


**Fig. 4.** Through-thickness variation in FGPM/homogeneous bi-layer sensory plate in (a) in-plane displacement ( $h_1=0.2h$ ), (b) in-plane displacement ( $h_1=0.8h$ ), (c) transverse displacement ( $h_1=0.2h$ ), (d) transverse displacement ( $h_1=0.8h$ ), (e) transverse normal stress ( $h_1=0.2h$ ), (f) transverse normal stress ( $h_1=0.8h$ )

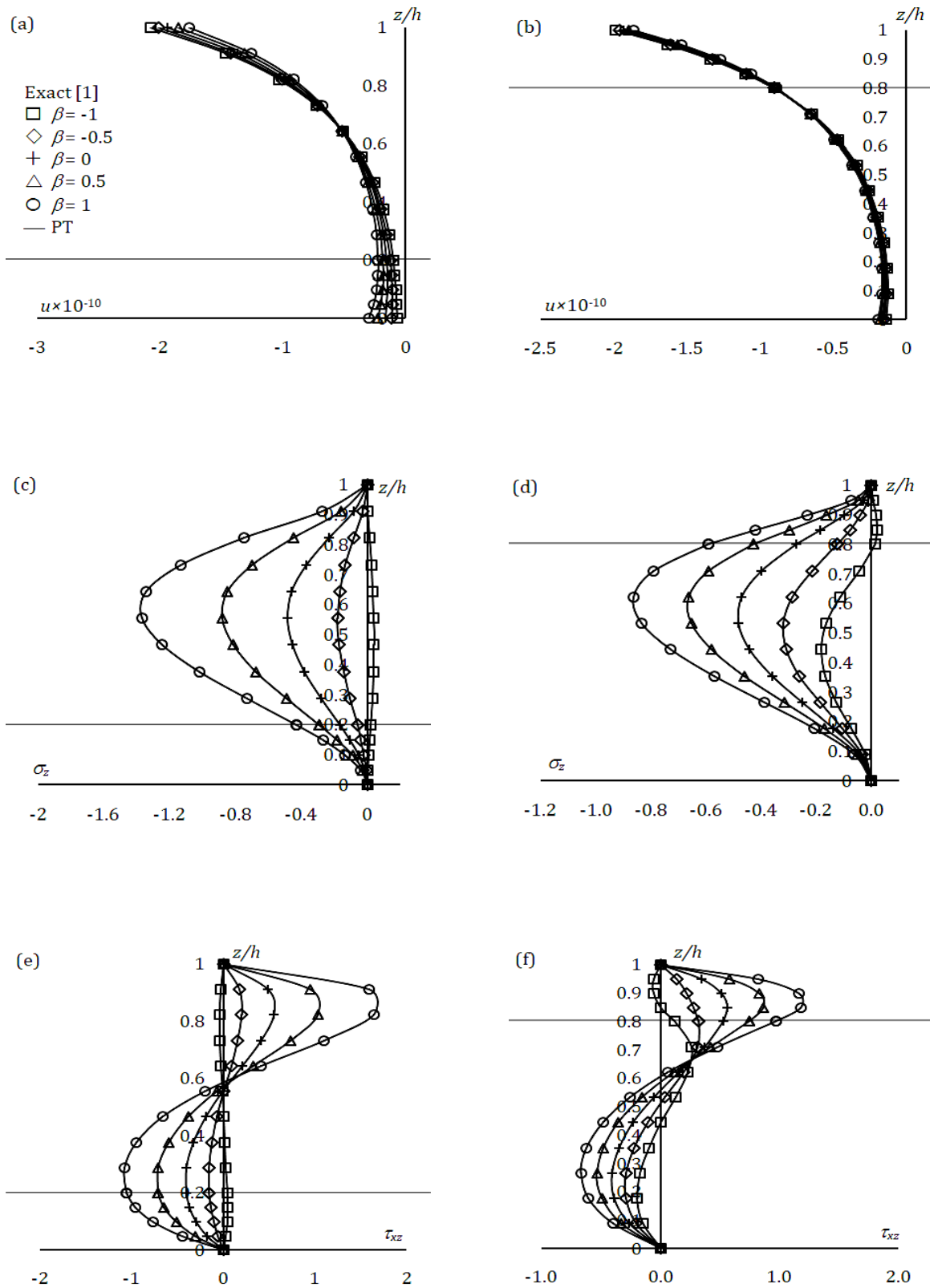


**Fig. 5.** Through-thickness variation in FGPM/homogeneous bi-layer actuating plate in (a) in-plane displacement ( $h_1=0.2h$ ), (b) in-plane displacement ( $h_1=0.8h$ ), (c) transverse normal stress ( $h_1=0.2h$ ), (d) transverse normal stress ( $h_1=0.8h$ ), (e) transverse shear stress ( $h_1=0.2h$ ), (f) transverse shear stress ( $h_1=0.8h$ )

**Table 2.** Displacements and stresses in a simply supported sensory PVDF beam under sinusoidal mechanical loading

Entity	z	Gradation Constant $\beta$				
		-1	-0.5	0	0.5	1
$u \times 10^{-10}$	0	1.207	1.023	0.8647	0.7288	0.6118
	0.5h	-0.229	-0.088	0.0029	0.058	0.088
	h	-1.649	-1.193	-0.8594	-0.6171	-0.4421
$w \times 10^{-9}$	0	0.9842	0.7637	0.594	0.4632	0.3621
	0.5h	0.9874	0.7667	0.5968	0.4657	0.3643
	h	0.9824	0.7633	0.5945	0.4642	0.3634
$\phi \times 10^{-3}$	0.5h	2	1.6	1.3	0.9966	0.7375
$\tau_{xz}$	0.5h	4.6944	4.7403	4.7557	4.7403	4.6942
$\sigma_z$	0.5h	0.5636	0.5318	0.5	0.4681	0.4362
$D_z \times 10^{-10}$	0	-0.2002	-0.1516	-0.0998	-0.0482	0.0001
	0.5h	-0.2314	-0.1811	-0.1276	-0.0741	-0.02376
	h	-0.2553	-0.207	-0.1554	-0.1037	-0.05505
$\sigma_x$	0	-31.7027	-44.3007	-61.7555	-85.815	-118.761
	0.5h	7.9285	5.7398	1.723	-4.9053	-15.1802
	h	43.3258	51.6678	61.3678	72.6612	85.8278

**Table 3.** Displacements and stresses in a simply supported actuating PVDF beam under sinusoidal electric loading

Entity	z	Gradation Constant $\beta$				
		-1	-0.5	0	0.5	1
$u \times 10^{-11}$	0	-0.1621	-0.2249	-0.2924	-0.36	-0.4231
	0.5h	-0.219	-0.2183	-0.218	-0.2183	-0.219
	h	-0.4341	-0.3716	-0.3041	-0.2365	-0.1733
$w \times 10^{-10}$	0	0.0001	-0.0482	-0.0998	-0.1516	-0.2002
	0.5h	0.0954	0.0623	0.0263	-0.0097	-0.0431
	h	0.2553	0.207	0.1554	0.1037	0.055
$\phi$	0.5h	0.3733	0.4328	0.4943	0.5558	0.6155
$\tau_{xz}$	0.5h	0.0005	0.0004	0	-0.0009	-0.0015
$\sigma_z \times 10^{-3}$	0.5h	-0.3912	-0.7791	-1.1	-1.3	-1.1
	0	-0.6493	-0.8598	-1.115	-1.418	-1.765
$D_z \times 10^{-8}$	0.5h	-0.6557	-0.8689	-1.128	-1.435	-1.789
	h	-0.6715	-0.8939	-1.167	-1.496	-1.883
	0	-0.5749	-0.3509	0.3685	2.0541	5.4925
$\sigma_x$	0.5h	-0.4352	-0.3935	-0.1823	0.3577	1.4922
	h	0.1054	0.2315	0.372	0.4787	0.4619

**Table 4.** Displacements and stresses in a simply supported sensory PVDF beam under uniformly distributed mechanical loading

Entity	Location	Gradation Factor $\beta$				
		-1	-0.5	0	0.5	1
$u \times 10^{-10}$	+ h/2	-2.1305211	-1.5619067	-1.0758951	-0.8027623	-0.5814465
$w \times 10^{-10}$	+ h/2	12.6232173	9.80410553	7.64594844	5.96345347	4.66761745
$\phi \times 10^{-3}$	0	3.09304359	2.4978856	2.0161351	1.53476254	1.13796579
$\tau_{xz}$	0	7.10130203	7.1779797	7.2132	7.15415914	7.18174222
$\sigma_z$	0	1.43362666	1.35486238	1.2848	1.14052316	1.18774109
$D_z \times 10^{-11}$	+ h/2	-6.008076	-4.783087	-6.45538	-3.183497	-2.780888
	- h/2	-42.8965	-59.8896	-83.3995	-115.6573	-160.1848
$\sigma_x$	0	10.745	7.7635	2.3014	-6.6394	-20.6428
	h/2	57.168	83.5723	35.2159	106.0003	143.5741

**Table 5.** Displacements and stresses in a simply supported actuating PVDF beam under uniformly distributed electric loading

Entity	Location	Gradation Factor $\beta$				
		-1	-0.5	0	0.5	1
$u \times 10^{-11}$	$+ h/2$	-1.584256	-0.9602038	-10.690703	1.1152712	1.06158
$w \times 10^{-11}$	$+ h/2$	6.388092	5.68934	2.77707	4.47325	3.019088
$\phi$	0	0.8052	0.9329	1.0635	1.1968	1.3266
	$-h/4$	-0.8876	-1.2576	-1.8416	-1.9147	-2.4401
$\tau_{xz}$	0	0.0091	-0.1522	-0.7494	-0.3334	-1.0751
	$+h/4$	1.6587	2.4391	2.3543	5.0003	5.5395
	0	-0.8566981	-1.3580919	-2.8218	-1.8717	-8.8592
$D_z \times 10^{-8}$	$+ h/2$	-2.90026	-4.21218	-6.05078	-8.87531	-12.85177
	$- h/2$	0.8807	3.553	9.6994	19.713	40.7047
$\sigma_x$	0	-1.7939	-2.2672	-2.3797	-3.1374	-2.0641
	$+ h/2$	34.5471	14.6918	4.3232	47.4725	53.3201

**Example 5**

A simply supported hybrid beam of thickness  $h$  consisting of Ni and  $Al_2O_3$  bi-material functionally gradient elastic substrate with a piezoelectric layer of PZT-5A of thickness  $0.1h$  bonded to its ceramic-rich top surface is considered. The FGM substrate comprises a 100% metal layer of thickness  $0.1h_e$  and nine perfectly bonded isotropic layers of equal thickness (Figure 6) with different material properties computed at the mid-surface of the respective layers. The volume fractions  $V_c$  and  $V_m$  of the ceramic and metal are assumed to vary along the thickness using the power law as;

$$\begin{aligned}
 V_m(z) &= 1 - (z/h + 0.5)^M; M \geq 1 \\
 V_m(z) &= 1 - (z/h + 0.5)^{1/M}; M \leq 1 \\
 V_c(z) &= 1 - V_m(z)
 \end{aligned}
 \tag{14}$$

$M = 0.25, 4$  is the in-homogeneity parameter. Effective Young's modulus for FGM is obtained as;

$$Y = \frac{V_m Y_m (q + Y_c) / (q + Y_m) + (1 - V_m) Y_c}{V_m (q + Y_c) / (q + Y_m) + (1 - V_m)}
 \tag{15}$$

where  $q = 4.5$  GPa for Ni- $Al_2O_3$ . Properties of Ni,  $Al_2O_3$ , and PZT-5A are given in Table 1. For FGM substrate, piezoelectric stress constants  $e_{ij}$  in Eq. (9) are made zero.

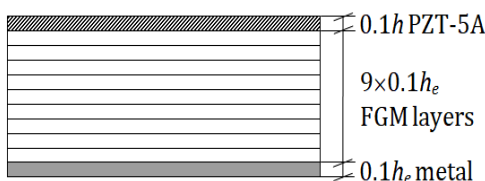


**Fig. 6.** Hybrid Beam Configuration

Three aspect ratios  $S = a/h = 5, 10, 40$  are investigated. The hybrid beam is subjected to the following two loading cases;

1. Mechanical load at the upper surface;

$$p = -1 \sin\left(\frac{\pi x}{a}\right) \text{ with open circuit condition, i.e.,}$$

$D_z = 0$ , and the results are normalized as;

$$\begin{aligned}
 (\bar{u}, \bar{w}) &= 100(u, w / S) Y_0 / h S^3 p_0, \\
 (\bar{\sigma}_x, \bar{\tau}_{xz}) &= (\sigma_x / S, 100 \tau_{xz}) / S p_0,
 \end{aligned}
 \tag{16}$$

$$\bar{\varphi} = 10^4 \varphi Y_0 d_0 / h S^2 p_0$$

2. Applied actuation potential at the upper surface;  $\varphi = 1 \sin\left(\frac{\pi x}{a}\right)$  with traction-free upper and lower face and the results are normalized as;

$$\begin{aligned}
 (\bar{u}, \bar{w}) &= 10(Su, w) / S^2 d_0 \varphi_0, \\
 (\bar{\sigma}_x, \bar{\tau}_{xz}) &= (0.1 \sigma_x, 100 S \tau_{xz}) h / Y_0 d_0 \varphi_0,
 \end{aligned}
 \tag{17}$$

$$\bar{D}_z = h D_z / 10 Y_0 d_0^2 \varphi_0$$

where  $Y_0 = 199.5$  GPa,  $d_0 = 374 \times 10^{-12}$  CN<sup>-1</sup>.

Comparison of results obtained by the present model with exact theory and a few approximate theories like Zigzag theory (ZIGT), Consistent third-order theory (CTOT), First-order shear deformation theory (FSDT) given by Kapuria et al. [44] is shown in Table 6 for loading case 1 and Table 7 for loading case 2. It can be seen that the present model is performing quite efficiently.

**Table 6.** Exact 2D results and percentage error in Present theory, ZIGT, CTOT, FSDT results in hybrid beam for  $M = 0.25$  (\*Reference [44])

Entity	S	Load Case 1					Load Case 2				
		Exact <sup>a</sup>	Present	ZIGT <sup>a</sup>	CTOT <sup>a</sup>	FSDT <sup>a</sup>	Exact <sup>a</sup>	Present	ZIGT <sup>a</sup>	CTOT <sup>a</sup>	FSDT <sup>a</sup>
$w$	5	-10.897	0.68	1.71	1.3	1.74	0.77736	0.244	0.26	0.51	-1.21
	10	-10.448	-0.38	0.45	0.34	0.46	0.77509	0.054	0.07	0.13	-0.3
	40	-10.308	-0.08	0.03	0.02	0.03	0.77438	-0.006	0	0.01	-0.02
$10\sigma_x^e$	5	8.2616	0	1.03	0.96	-0.62	0.47717	-0.886	-0.87	8.02	-1.98
	10	8.2241	-0.18	0.25	0.31	-0.17	0.47008	-0.206	-0.22	2.03	-0.5
	40	8.2112	-0.01	0.02	0.01	-0.01	0.46786	-0.016	-0.01	0.13	-0.03
$\sigma_x^p$	5	-0.2048	-0.19	-5.16	-2.2	-3.16	-0.12517	0.124	0.14	-0.89	0.27
	10	-0.20014	-0.44	-1.41	-0.65	-0.9	-0.12549	0.004	0.02	-0.24	0.06
	40	-0.19876	-0.21	-0.24	-0.19	-0.21	-0.12559	-0.016	-0.02	-0.03	-0.02
$\tau_{xz}$	5	-52.463	-0.07	0.26	0.14	0.36	-38.779	0.314	0.33	-1.07	0.72
	10	-52.607	-0.04	0.06	0.03	0.09	-38.99	0.064	0.08	-0.27	0.18
	40	-52.65	-0.03	0	0	0.01	-39.056	-0.006	0.01	-0.02	0.01
$\phi/D_z$	5	55.039	-1.03	-1.08	8.39	8.06	-0.77318	-0.066	-0.05	0.07	-0.12
	10	88.986	-0.69	-1.66	13	12.5	-0.77204	-0.006	0	0.03	-0.02
	40	99.635	-0.12	-0.09	0.73	0.4	-0.77169	0.004	0.02	0.02	0.02

**Table 7.** Exact 2D results and percentage error in Present theory, ZIGT and CTOT results in hybrid beam for  $M = 4$  (\*Reference [44])

Entity	S	Load Case 1				Load Case 2			
		Exact <sup>a</sup>	Present	ZIGT <sup>a</sup>	CTOT <sup>a</sup>	Exact <sup>a</sup>	Present	ZIGT <sup>a</sup>	CTOT <sup>a</sup>
$w$	5	-13.576	0.786	1.52	1.07	0.91689	0.178	0.18	1
	10	-12.791	-0.134	0.4	0.27	0.90965	0.048	0.05	0.25
	40	-12.544	-0.04	0.03	0.02	0.90738	-0.002	0	0.02
$10\sigma_x^e$	5	8.885	-0.024	0.71	0.53	0.56323	-0.112	-0.51	6.02
	10	8.8007	-0.14	0.17	0.12	0.55734	-0.102	-0.13	1.52
	40	8.7728	-0.024	0.01	0.01	0.5555	-0.012	-0.01	0.1
$\sigma_x^p$	5	-0.24047	-1.674	-3.94	-1.8	-0.12256	0.098	0.1	-0.82
	10	-0.23491	-1.034	-1.1	-0.55	-0.12284	0.008	0.01	-0.22
	40	-0.23327	-0.164	-0.23	-0.19	-0.12293	-0.02	-0.02	-0.04
$\tau_{xz}$	5	-49.19	-0.024	0.11	0.09	-37.892	0.298	0.3	-1
	10	-49.35	-0.004	0.03	0.02	-38.089	0.078	0.08	-0.25
	40	-49.399	0	0	0	-38.151	0.008	0.01	-0.02
$\phi/D_z$	5	723.27	-0.154	-7.42	65.5	-0.77447	-0.005	-0.05	0.07
	10	1060.7	-1.174	-1.24	11.2	-0.77335	0	0	0.03
	40	1166.6	-0.004	-0.07	0.63	-0.77301	0.018	0.02	0.02

### 5. Conclusions

A Semi-analytical formulation for electro-mechanical analysis of simply supported FGPM laminate in cylindrical bending has been developed. The formulation is based upon elasticity theory with no simplifying assumption on stress and displacement fields. Solutions are obtained using numerical integration. The model is computationally inexpensive and versatile. By appropriate substitution of material property coefficients and the gradation law, it may be used for homogeneous, grading stiff, grading soft, and sandwich plates. The approach may be extended for clamped-clamped BCs but not for arbitrary BCs. Results obtained by the present formulation are in very good agreement with the exact results. A few other results and observations have been noted for future reference.

### Nomenclature

$a, b, h$	Length, breadth, and depth of plate
$C^E$	Elasticity coefficients at constant electric field
$E_1, E_3$	Elastic moduli in principal directions
$g^S$	Dielectric constants at constant strain
$\nu_{ij}$ $i, j=1, 3$	Generalized Poisson's ratios
$u, w$	$x$ and $z$ direction displacements
$\sigma_x, \sigma_z$	Normal stress in $x$ and $z$ direction
$\tau_{xz}$	Shear stress in $xz$ plane
$\epsilon_x, \epsilon_z$	Normal strain in $x$ and $z$ direction
$\gamma_{xz}$	Shear strain in $x$ - $z$ plane
$C_{ij}$ $i, j=1, 2, \dots, 6$	Material stiffness coefficients
$E_x, E_z$	Electric field intensities in $x$ and $z$ directions
$e_{ij}$ $i, j=1, 2, \dots, 6$	Piezoelectric constants
$g_{ii}$ $i=1, 2, 3$	Dielectric constants
$D_x, D_z$	Electric displacements in $x$ and $z$ directions
$B_x, B_z$	Body force intensities in $x$ and $z$ directions

### Appendix

The vectors and matrices in Eqs. (2) are as follows;

$$\text{Stress vector; } \{\sigma\} = \begin{Bmatrix} \sigma_x \\ \sigma_z \\ \tau_{xz} \end{Bmatrix} \quad (18)$$

$$\text{Strain vector; } \{\epsilon\} = \begin{Bmatrix} \epsilon_x \\ \epsilon_z \\ \gamma_{xz} \end{Bmatrix} \quad (19)$$

Stiffness matrix at the constant electric field;

$$[C^E] = \begin{bmatrix} C_{11} & C_{13} & 0 \\ C_{31} & C_{33} & 0 \\ 0 & 0 & C_{55} \end{bmatrix} \quad (20)$$

in which the reduced material coefficients  $C_{ij}$  in plane stress condition of elasticity are;

$$C_{11} = \frac{E_1}{1 - \nu_{13}\nu_{31}}, \quad C_{13} = C_{31} = \frac{\nu_{13}E_1}{1 - \nu_{13}\nu_{31}}, \quad (21)$$

$$C_{33} = \frac{E_3}{1 - \nu_{13}\nu_{31}}, \quad C_{55} = G_{13}$$

and in-plane strain condition of elasticity;

$$C_{11} = \frac{E_1(1 - \nu_{23}\nu_{32})}{\Delta},$$

$$C_{13} = C_{31} = \frac{E_1(\nu_{31} + \nu_{21}\nu_{32})}{\Delta}, \quad (22)$$

$$C_{33} = \frac{E_3(1 - \nu_{12}\nu_{21})}{\Delta}; \quad C_{55} = G_{13},$$

$$\Delta = (1 - \nu_{12}\nu_{21} - \nu_{23}\nu_{32} - \nu_{31}\nu_{13} - 2\nu_{12}\nu_{23}\nu_{31})$$

Piezoelectric stress constants matrix due to Cady [45] and dielectric constant matrix at constant strain due to Tzau and Pandita [46] are respectively;

$$[e] = \begin{bmatrix} 0 & 0 & e_{31} \\ 0 & 0 & e_{33} \\ e_{15} & 0 & 0 \end{bmatrix} \quad (23)$$

$$[g^S] = \begin{bmatrix} g_{11} & 0 & 0 \\ 0 & 0 & 0 \\ 0 & 0 & g_{33} \end{bmatrix} \quad (24)$$

The electric field intensity vector and electric displacement vector are respectively;

$$\{E\} = \begin{Bmatrix} -\partial\phi/\partial x \\ 0 \\ -\partial\phi/\partial z \end{Bmatrix} \quad (25)$$

$$\{D\} = \begin{Bmatrix} D_x \\ 0 \\ D_z \end{Bmatrix} \quad (26)$$

The electro-elastic coefficients  $Q_{11} - Q_{66}$  in Eqs. (9) are as below;

$$\begin{aligned}
 Q_{11} &= Q_{15} = Q_{16} = 0, \\
 Q_{22} &= Q_{23} = Q_{24} = 0, \\
 Q_{32} &= Q_{33} = Q_{34} = 0, \\
 Q_{42} &= Q_{43} = Q_{44} = 0, \\
 Q_{51} &= Q_{52} = Q_{53} = Q_{55} = Q_{56} = 0, \\
 Q_{61} &= Q_{62} = Q_{65} = Q_{66} = 0 \\
 \\
 Q_{12} &= -\alpha_m, \quad Q_{13} = -\left(\frac{e_{15}^0}{C_{55}^0}\right)\alpha_m, \\
 \\
 Q_{14} &= \left(\frac{1}{f(z)C_{55}^0}\right)\tau_{xzm}, \\
 \\
 Q_{21} &= \left(\frac{g_{33}^0 C_{31}^0 + e_{33}^0 e_{31}^0}{C_{33}^0 g_{33}^0 + e_{33}^0 e_{33}^0}\right)\alpha_m, \\
 \\
 Q_{25} &= \frac{1}{f(z)}\left(\frac{g_{33}^0}{C_{33}^0 g_{33}^0 + e_{33}^0 e_{33}^0}\right), \\
 \\
 Q_{26} &= \frac{1}{f(z)}\left(\frac{e_{33}^0}{C_{33}^0 g_{33}^0 + e_{33}^0 e_{33}^0}\right)D_{zm}, \\
 \\
 Q_{31} &= -\left(\frac{C_{33}^0 e_{31}^0 - e_{33}^0 C_{31}^0}{C_{33}^0 g_{33}^0 + e_{33}^0 e_{33}^0}\right)\alpha_m, \\
 \\
 Q_{35} &= \frac{1}{f(z)}\left(\frac{e_{33}^0}{C_{33}^0 g_{33}^0 + e_{33}^0 e_{33}^0}\right), \\
 \\
 Q_{36} &= -\frac{1}{f(z)}\left(\frac{C_{33}^0}{C_{33}^0 g_{33}^0 + e_{33}^0 e_{33}^0}\right), \\
 \\
 Q_{41} &= f(z)\left[\begin{array}{l} C_{11}^0 - \frac{C_{13}^0 g_{33}^0 C_{31}^0}{C_{33}^0 g_{33}^0 + e_{33}^0 e_{33}^0} \\ - \frac{e_{33}^0 C_{13}^0 e_{31}^0}{C_{33}^0 g_{33}^0 + e_{33}^0 e_{33}^0} \\ + \frac{e_{31}^0 C_{33}^0 e_{31}^0 - e_{31}^0 C_{31}^0 e_{33}^0}{C_{33}^0 g_{33}^0 + e_{33}^0 e_{33}^0} \end{array}\right]\alpha_m^2, \\
 \\
 Q_{45} &= -\left(\frac{C_{13}^0 e_{33}^0 + e_{31}^0 e_{33}^0}{C_{33}^0 g_{33}^0 + e_{33}^0 e_{33}^0}\right)\alpha_m, \\
 \\
 Q_{46} &= -\left(\frac{C_{13}^0 e_{33}^0 - e_{31}^0 C_{33}^0}{C_{33}^0 g_{33}^0 + e_{33}^0 e_{33}^0}\right)\alpha_m, \quad Q_{54} = \alpha_m, \\
 \\
 Q_{63} &= -f(z)\left(\frac{e_{15}^0 e_{15}^0}{C_{55}^0} + g_{11}^0\right)\alpha_m^2 \phi_m(z), \\
 \\
 Q_{64} &= \left(\frac{e_{15}^0}{C_{55}^0}\right)\alpha_m
 \end{aligned} \tag{27}$$

**References**

[1] Lu P., Lee H.P. and Lu C., 2005. An exact solution for functionally graded piezoelectric laminates in cylindrical bending. *International Journal of Mechanical Sciences* 47(3), pp.437-458. DOI: 10.1016/j.ijmecsci.2005.01.012

[2] Lu P., Lee H.P. and Lu C., 2006. Exact solution for simply supported functionally graded piezoelectric laminates by Stroh-like formalism. *Composite Structures* 72(3), pp.352-363. DOI: 10.1016/j.compstruct.2005.01.012

[3] Xiang H.J. and Shi Z.F., 2009. Static analysis for functionally graded piezoelectric actuators or sensors under a combined electro-thermal load. *European Journal of Mechanics-A/Solids* 28(2), pp.338-346. DOI: 10.1016/j.euromechsol.2008.06.007

[4] Mikaeeli S. and Behjat B., 2016. Three-dimensional analysis of thick functionally graded piezoelectric plate using EFG method. *Composite Structures* 154, pp.591-599. DOI: 10.1016/j.compstruct.2016.07.067

[5] Kulikov G. M. and Plotnikova S. V., 2013. A new approach to three-dimensional exact solutions for functionally graded piezoelectric laminated plates. *Composite Structures*, 106, pp.33-46. DOI: 10.1016/j.compstruct.2013.05.037

[6] Lim C.W. and He L.H., 2001. Exact solution of a compositionally graded piezoelectric layer under uniform stretch, bending and twisting. *International Journal of Mechanical Sciences* 43, pp.2479-2492. DOI: 10.1016/S0020-7403(01)00059-5

[7] Reddy J.N. and Cheng Z.Q., 2001. Three-dimensional thermo-mechanical deformations of functionally graded rectangular plates. *European Journal of Mechanics - A/Solids*, 20(5), pp.841-855. DOI:10.1016/S0997-7538(01)01174-3

[8] Zhong Z. and Shang E.T., 2005. Exact analysis of simply supported functionally graded piezo-thermo-electric plates. *Journal of Intelligent Material Systems and Structures* 16(7-8), pp.643-651. DOI: 10.1177/1045389X05050530.

[9] Almajid A., Taya M. and Hudnut S., 2001. Analysis of out of-plane displacement and stress field in a piezocomposite plate with functionally graded microstructure. *International Journal of Solids and Structures*, 38(19), pp.3377-3391. DOI:10.1016/S0020-7683(00)00264-X.

[10] Joshi S., Mukherjee A. and Schmauder S., 2003. Numerical characterization of functionally graded active materials under electrical and thermal fields. *Smart Materials and Structures*, 12(4), pp.571-579. DOI:10.1088/0964-1726/12/4/309.

[11] Taya M., Almajid A., Dunn M. and Takahashi H., 2003. Design of bimorph piezo-composite actuators with functionally graded microstructure. *Sensors and Actuators-A/*

- Physical*, 107(3), pp.248–260.  
DOI: 10.1016/S0924-4247(03)00381-9.
- [12] Zhong Z. and Yu T., 2007. Electroelastic analysis of functionally graded piezoelectric material beams. *Journal of Intelligent Material Systems and Structures*, 19(6), pp.707–713.  
DOI: 10.1177/1045389X07079453.
- [13] Wu D., Gao W., Hui D., Gao K. and Li K., 2018. Stochastic static analysis of Euler-Bernoulli type functionally graded structures. *Composites Part B/Engineering*, 134, pp.69–80.  
DOI: 10.1016/j.compositesb.2017.09.050.
- [14] Loja M. A. R., Mota Soares C. M. and Barbosa J. I., 2013. Analysis of functionally graded sandwich plate structures with piezoelectric skins, using B-spline finite strip method. *Composite Structures*, 96, pp.606–615.  
DOI: 10.1016/j.compstruct.2012.08.010.
- [15] Li Y. S., Feng W. J. and Cai Z. Y., 2014. Bending and free vibration of functionally graded piezoelectric beam based on modified strain gradient theory. *Composite Structures*, 115, pp.41–50.  
DOI: 10.1016/j.compstruct.2014.04.005.
- [16] Chuaqui T. R. C. and Roque C. M. C., 2017. Analysis of functionally graded piezoelectric Timoshenko smart beams using a multiquadric radial basis function method. *Composite Structures*, 176, pp.640–653.  
DOI: 10.1016/j.compstruct.2017.05.062.
- [17] Nourmohammadi H. and Behjat B., 2019. Static analysis of functionally graded piezoelectric plates under Electro-thermo-mechanical loading using a meshfree method based on RPIM. *Journal of Stress Analysis*, 4(2), pp.93–106.  
DOI: 10.22084/JRSTAN.2020.20850.1125.
- [18] Behjat B. and Khoshravan M. R., 2012. Geometrically nonlinear static and free vibration analysis of functionally graded piezoelectric plates. *Composite Structures*, 94(3), pp.874–882.  
DOI: 10.1016/j.compstruct.2011.08.024
- [19] Raissi H., 2020. Stress analysis in adhesive layers of a five-layer circular sandwich plate subjected to temperature gradient based on layerwise theory. *Mechanics Based Design of Structures and Machines*, pp.1–27.  
DOI: 10.1080/15397734.2020.1776619.
- [20] Raissi H., Shishehsaz M. and Moradi S., 2019. Stress distribution in a five-layer sandwich plate with FG face sheets using layerwise method. *Mechanics of Advanced Materials and Structures*, 26(14), pp.1234–1244.  
DOI: 10.1080/15376494.2018.1432796.
- [21] Raissi H., Shishehsaz M. and Moradi S., 2020. Stress analysis of the five-layer circular sandwich plate subjected to uniform distributed load by layerwise theory along with second order shear deformation theory. *Australian Journal of Mechanical Engineering*, pp.1–12.  
DOI: 10.1080/14484846.2020.1733170.
- [22] Song D and Luo N, 2012, Wave propagation and transient response of a functionally graded material plate under a point impact load in thermal environment. *Applied Mathematical Modelling*, 36, pp.444-462.  
DOI: 10.1016/j.apm.2011.07.023
- [23] Mazzotti M. Bartoli I. Miniaci M. Marzani A. 2016. Wave dispersion in thin-walled orthotropic waveguides using the first order shear deformation theory. *Thin-Walled Structures*, 103, pp.128-140.  
DOI: 10.1016/j.tws.2016.02.014
- [24] Li C.L., Han Q., Wang Z., Wu X., 2020, Analysis of wave propagation in functionally graded piezoelectric composite plates reinforced with graphene platelets. *Applied Mathematical Modelling*, 81, pp.487–505.  
DOI: 10.1016/j.apm.2020.01.016
- [25] Li C.L. and Han Q., 2020. Semi-analytical wave characteristics analysis of graphene-reinforced piezoelectric polymer nanocomposite cylindrical shells. *International Journal of Mechanical Sciences*, 186:105890.  
DOI: 10.1016/j.ijmecsci.2020.105890
- [26] Li C.L., Han Q., Y. J. Liu D. L. Xiao, 2017. Guided wave propagation in rotating functionally graded annular plates. *Acta Mechanica*, 228, pp.1083-1095.  
DOI: 10.1007/s00707-016-1752-9.
- [27] Vinh P.V. and Tounsi A., 2022. Free vibration analysis of functionally graded doubly curved nanoshells using nonlocal first-order shear deformation theory with variable nonlocal parameters. *Thin-Walled Structures*, 174.  
DOI: 10.1016/j.tws.2022.109084.
- [28] Tahir S.I., Tounsi A., Chikh A., Al-Osta M., Al-Dulaijan S.U. and Al-Zahrani M.M., The effect of three-variable viscoelastic foundation on the wave propagation in functionally graded sandwich plates via a simple quasi-3D HSDT. *Steel and Composite Structures* 42(4), pp.501-511.  
DOI:10.12989/scs.2022.42.4.501.
- [29] Rachid A., Ouinas D., Lousdad A., Zaoui F.Z., Achour B., Gasmi H., Butt T.A., Tounsi A., 2022. Mechanical behavior and free vibration analysis of FG doubly curved shells on elastic foundation via a new modified displacements field model of 2D and quasi-3D HSDTs. *Thin-Walled Structures*, 172.  
DOI: 10.1016/j.tws.2021.108783.
- [30] Habib H., Abdelbaki C., Bousahla A.A., Bourada F., 2022. Effect of the variable visco-

- Pasternak foundations on the bending and dynamic behaviors of FG plates using integral HSDT model. *Geomechanics and Engineering* 28(1), pp.49-64. DOI: 10.12989/gae.2022.28.1.049.
- [31] Bouafia K., Selim M. M., Bourada F., Bousahla A. A., Bourada M., Tounsi A., Bedia E. A. A., Tounsi A., 2021. Bending and free vibration characteristics of various compositions of FG plates on elastic foundation via quasi 3D HSDT model. *Steel and Composite Structures*, 41 (4), pp. 487-503. DOI: 10.12989/scs.2021.41.4.487.
- [32] Zaitoun M. W., Chikh A., Tounsi A., Al-Osta M. A., Sharif A., Al-Dulaijan S. U., Al-Zahrani M. M., 2022. Influence of the visco-Pasternak foundation parameters on the buckling behavior of a sandwich functional graded ceramic-metal plate in a hygrothermal environment. *Thin-Walled Structures*, 170. DOI: 10.1016/j.tws.2021.108549.
- [33] Mudhaffar I. M., Tounsi A., Chikh A., Al-Osta M. A., Al-Zahrani M. M. Al-Dulaijan S. U., 2021. Hygro-thermo-mechanical bending behavior of advanced functionally graded ceramic metal plate resting on a viscoelastic foundation. *Structures*, 33, pp.2177-2189. DOI: 10.1016/j.istruc.2021.05.090.
- [34] Kouider D, Kaci A, Selim M. M., Bousahla A. A., Bourada F., Tounsi, A., Tounsi A., Hussain M., 2021, An original four-variable quasi-3D shear deformation theory for the static and free vibration analysis of new type of sandwich plates with both FG face sheets and FGM hard core. *Steel and Composite Structures*, 41 (2), pp.167-191. DOI: 10.12989/scs.2021.41.2.167
- [35] Merazka B., Bouhadra A., Menasria A., Selim M. M., Bousahla A. A., Bourada F., Tounsi A., Benrahou K.H., Tounsi A. and Al-Zahrani M. M., 2021. Hygro-thermo-mechanical bending response of FG plates resting on elastic foundations. *Steel and Composite Structures*, 39 (5), pp.631-643. DOI: 10.12989/scs.2021.39.5.631.
- [36] Hachemi H., Bousahla A. A., Kaci A., Bourada F., Tounsi A., Benrahou K. H., Tounsi A., Al-Zahrani M. M. Mahmoud S. R., 2021. Bending analysis of functionally graded plates using a new refined quasi-3D shear deformation theory and the concept of the neutral surface position. *Steel and Composite Structures*, 39 (1), pp.51-64. DOI: 10.12989/scs.2021.39.1.051
- [37] Bakoura A., Bourada F., Bousahla A. A., Tounsi A., Benrahou K. H., Tounsi A., Al-Zahrani M. M., Mahmoud S. R., 2021. Buckling analysis of functionally graded plates using HSDT in conjunction with the stress function method. *Computers and Concrete*, 27 (1), pp. 73-83. DOI: 10.12989/cac.2021.27.1.073.
- [38] Tiersten H.F., 1969. *Linear piezoelectric plate vibrations*. Plenum Press New York.
- [39] Maxwell J.C., 1865. A dynamical theory of the electromagnetic field. *Royal Society Transactions* 155, pp.459-512. DOI: 10.1098/rstl.1865.0008
- [40] Kantorovich L.V. and Krylov V.I., 1964. *Approximate methods of higher analysis*. Interscience Publishers, Inc. New York.
- [41] Kant T. and Ramesh C.K., 1981. Numerical integration of linear boundary value problems in solid mechanics by segmentation method. *International Journal of Numerical Methods in Engineering* 17, pp.1233-1256. DOI: 10.1002/nme.1620170808
- [42] Sawarkar S.S., Pendhari S.S. and Desai Y.M. 2016. Semi-analytical solutions for static analysis of piezoelectric laminates. *Composite Structures* 153, pp.242-252. DOI: 10.1016/j.compstruct.2016.05.106.
- [43] Heylinger P.R., Ramirez G. and Pei K.C., 1994. *Discrete layer piezoelectric plate and shell models for active tip-clearance control*. NASA Contractor Report, 195383.
- [44] Kapuria S., Bhattacharyya M. and Kumar A.N., 2006. Assessment of coupled 1D models for hybrid piezoelectric layered functionally graded beams. *Composite Structures* 72(4), pp.455-468. DOI: 10.1016/j.compstruct.2005.01.015
- [45] Cady W.G., 1946. *Piezoelectricity I & II*. Dover Publications New York.
- [46] Tzau H.S. and Pandita S., 1987. A multipurpose dynamic and tactile sensor for robot manipulators. *Journal of Robotic Systems* 4, pp.719-741.